Faculty Publications

Biology

2013

Flagellar Waveform Dynamics of Freely Swimming Algal Cells

H. Kurtuldu

D. Tam

A. E. Hosoi

Karl A. Johnson
Haverford College, kjohnson@haverford.edu

Follow this and additional works at: http://scholarship.haverford.edu/biology_facpubs

Flagellar waveform dynamics of freely swimming algal cells

H. Kurtuldu,[1] D. Tam,[2] A. E. Hosoi,[3] K. A. Johnson,[4,*] and J. P. Gollub[1,5]

[1]*Department of Physics, Haverford College, Haverford, Pennsylvania 19041, USA*
[2]*Laboratory for Aero and Hydrodynamics, Delft University of Technology, 2628CJ Delft, The Netherlands*
[3]*Department of Mechanical Engineering, Massachusetts Institute of Technology, Massachusetts 02139, USA*
[4]*Department of Biology, Haverford College, Haverford, Pennsylvania 19041, USA*
[5]*Department of Physics, University of Pennsylvania, Philadelphia, Pennsylvania 11904, USA*

We present quantitative measurements of time-dependent flagellar waveforms for freely swimming biflagellated algal cells, for both synchronous and asynchronous beating. We use the waveforms in conjunction with resistive force theory as well as a singularity method to predict a cell's time-dependent velocity for comparison with experiments. While net propulsion is thought to arise from asymmetry between the power and recovery strokes, we show that hydrodynamic interactions between the flagella and cell body on the return stroke make an important contribution to enhance net forward motion.

I. INTRODUCTION

Flagella, micron-sized appendages of many eukaryotic cells, play a critical role in locomotion and biological fluid flows [1,2]. Eukaryotic flagella and structurally similar cilia [3] contain an array of microtubules organized into an axoneme. Flagella are driven by dynein molecular motors that hydrolyze ATP to "walk" along one microtubule while attached to a neighbor, generating stress leading to bending. Ciliary motility is essential for human life; defects in flagellar (ciliary) function can result in a variety of human diseases such as infertility, cystic kidney disease, and retinal dystrophy [4]. For decades, the eukaryotic green alga *Chlamydomonas* [5] has been used as a model organism for studies of flagellar motility [6,7]. Much remains to be learned experimentally about the dynamics of flagella on freely swimming cells.

Chlamydomonas reinhardtii is a single cell with a body diameter of $\sim$10 μm and two anterior flagella each 10–15 μm in length. It swims at low Reynolds number (Re $\sim$$10^{-2}$), where viscous effects dominate inertia; therefore, the total net force and torque on the cell body can be assumed to vanish at any instant in the absence of an external force [8]. For instance, an algal cell would come to a complete stop in $\sim$0.1 ms if the flagella were to stop beating [9]. Cylindrical (radius $r \cong 125$ nm) flagella beat with a waveform that apparently optimizes the swimming efficiency [10]. Net forward motion is achieved by coordinated beating of the twin flagella at 45–60 Hz in a breaststroke motion, which propels the organism at a mean speed of 100–200 μm/s [11]. *C. reinhardtii* can vary the beat frequency of its flagella to switch between synchronous and asynchronous beating states [6,7] and change direction, thus, producing a random walk [12–14].

This paper presents the first quantitative experimental measurements of the time-dependent deformations of the flagella (including local curvature and local velocity) of freely swimming biflagellated cells, in both synchronous and asynchronous states. Here, the detailed information on the flagellar deformations first is used to identify the structure of the stroke as a traveling wave of curvature propagating along the flagellum. The experimental data further allow us to characterize the desynchronization events between the two flagella. Finally, we use measurements of both the flagellar deformations and the instantaneous velocity of the cell to demonstrate that the generation of forward motion crucially depends on hydrodynamic interactions between cell and flagella.

II. QUANTITATIVE MEASUREMENTS OF FLAGELLA ON FREELY SWIMMING CELLS

Experiments are performed using a microscope and a high-speed camera to capture the motion of the cells swimming in a thin film with a thickness of $h \approx 15$ μm, about 1.5–2.0 times the body diameter, so cells cannot rotate about their swimming axis (for details, see Ref. [15]). Although we have recorded data for hundreds of cells, in only a small fraction of cases do the full lengths of both flagella remain in focus for complete beat cycles and, thus, are suitable for quantitative analysis. The depth of field of the 40$\times$, 0.75 N.A. objective used in this study is less that 1 μm (1/15th of the thin film thickness); as a consequence, the flagellar contours are 2D projections that closely approximate the actual 3D waveforms. Applying these stringent criteria to data collected from freely swimming cells, we have been able to fully analyze the flagellar contours for about 10 complete cycles. Microscope images are preprocessed using digital Fourier filters to minimize halo artifacts surrounding the cell. After intensity thresholding, the pixels belonging to each flagellum are determined based on their locations and are then tracked from the point of body attachment to the tip of the flagellum. The center line of each flagellum in each frame is found using a 6th order polynomial fit to the parametrized pixel locations (for a similar analysis, see Ref. [16]). The center-line points $\mathbf{r}(s,t)$ are then used to calculate the local velocities $\mathbf{V}(s,t) = \partial \mathbf{r}/\partial t$ of the flagellum as a function of time t and arc length s (in the laboratory frame of reference). An elliptical fit is used to determine the body center for the measurement of cell velocity $\mathbf{U}(t)$, and to determine the length of the semimajor and semiminor axes a,b

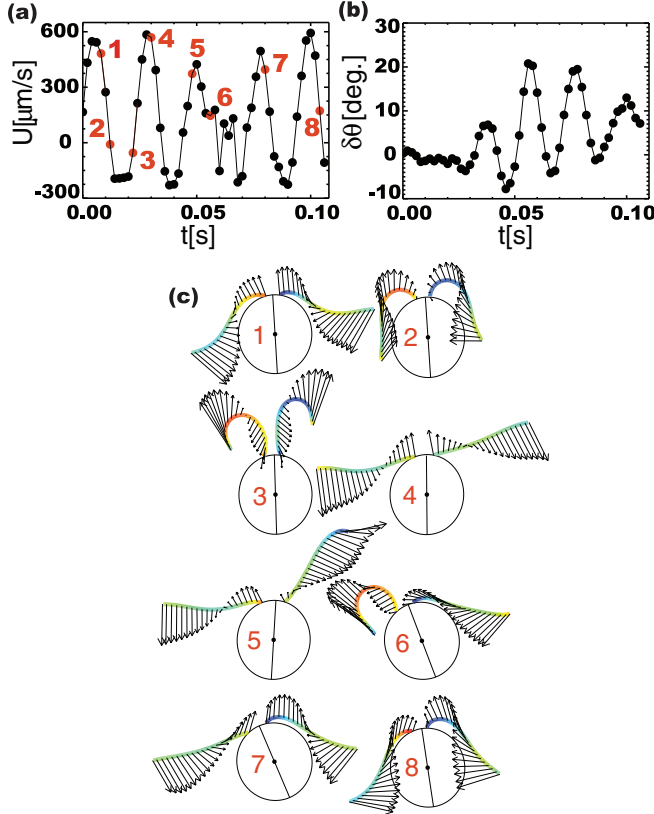*Corresponding author: kjohnson@haverford.edu

FIG. 1. (Color online) The body velocity (a) and instantaneous body angle change (b) as a function of time for a cell demonstrating both synchronous and asynchronous beating. (c) Flagellar waveforms at several instants, with curvature (color-coded as in Fig. 2) and vectors showing the time-dependent velocity **V** along each flagellum. (For movies, see Ref. [15].)
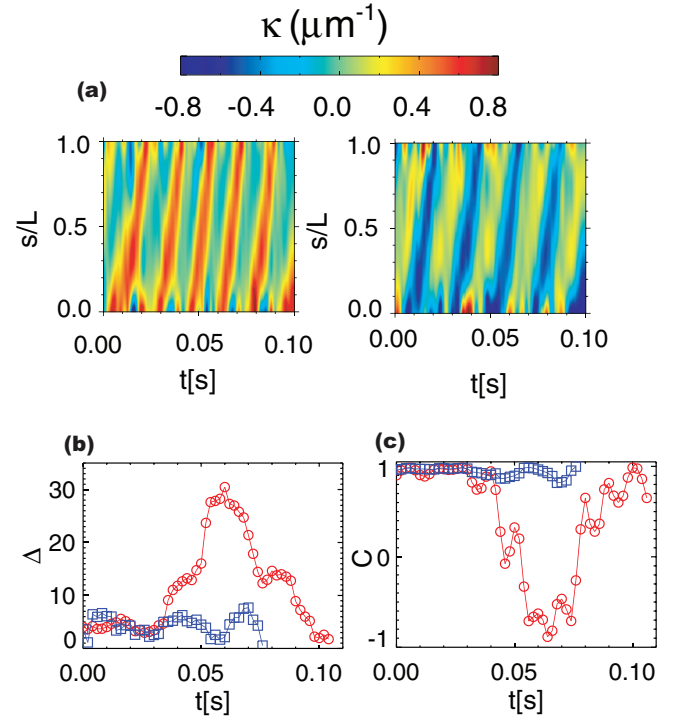

FIG. 2. (Color online) (a) Representative space-time curvature plots along the center line of each flagellum for a single cell, using opposite signs for the two flagella. Propagating waves are evident. (b) The normalized mean square net curvature Δ, averaged over the flagellar length, and (c) the velocity correlation C (see text) are shown as a function of time for two different cells, one showing asynchronous motion near 0.05 s (circles) and the other showing only synchronous motion (squares). (See additional figure in Ref. [15].)

of the cell body, as well as the body frame coordinate system $(x_\parallel, x_\perp)$ relative to the cell's axis.

In Fig. 1, flagellar waveforms at several instants designated 1–8 are shown for a cell demonstrating first synchronous and then asynchronous beating along with the corresponding instantaneous cell body velocity, and the body angle change with respect to the initial instant. For synchronized motion (1–4), the cell first extends its flagella and then sweeps them rearward to pull its body forward (power stroke, e.g., 4), while during the backward motion of the cell (recovery stroke, e.g., 2) it moves them closer to the body in the direction opposite to its movement, apparently reducing the body displacement in the reverse direction. The tips of the flagella move with a speed of ∼1 mm/s during the power and recovery stroke. The oscillatory behavior of the cell is interrupted when the two flagella become asynchronous (near ∼0.05 s); the cell body starts to wobble (4–7) as two flagella beat at different frequencies. This desynchronization event lasts ∼40 ms, and it causes the cell to change its orientation by ∼8° (see video in Ref. [15].) A longer interval of asynchronous motion could produce a larger angle change, as suggested by observations of less frequent but more extended periods of flagellar phase difference drifts on cells anchored to micropipettes [12].

Figure 2(a) represents measurements of the time-dependent curvature $\kappa(s,t)$ along the centerline of two flagella beating

at different frequencies. The data on curvature shows that the power and recovery strokes performed by the two flagella each consists of a single finite region of high curvature of constant sign and amplitude propagating from the base to the tip of the flagella at a constant speed. This propagation speed of the curvature can be calculated from the displacements of each curvature peak. We find wave speeds of 885 and 802 μm/s for the two flagella (with a standard deviation of the slope less than 20 μm/s). The periodic generation of these bending waves supports models of active bending [17], in which the microtubules on one side of the axoneme slide relative to the other. The magnitude of the displacement is measured to be about 400 nm.

III. CHARACTERIZATION OF DESYNCHRONIZATION EVENTS

We further characterize quantitatively the desynchronization events by two different methods. First, we compute the normalized net curvature $\Delta(t) = L^2 \langle (\kappa_1 + \kappa_2)^2 \rangle$, where κ is the signed local curvature of each flagellum (1, 2), and the brackets indicate averaging over the flagellar length L; Δ is defined to vanish in the symmetric synchronous state. We also consider the velocity correlation along the two flagella $C(t) = \langle V_{1,\parallel} V_{2,\parallel} \rangle / (\langle V_{1,\parallel}^2 \rangle \langle V_{2,\parallel}^2 \rangle)^{1/2}$, where $V_\parallel$ is the projection of the velocity along the major axis in the body frame. As shown in Figs. 2(b) and 2(c) both measures provide a clear signature
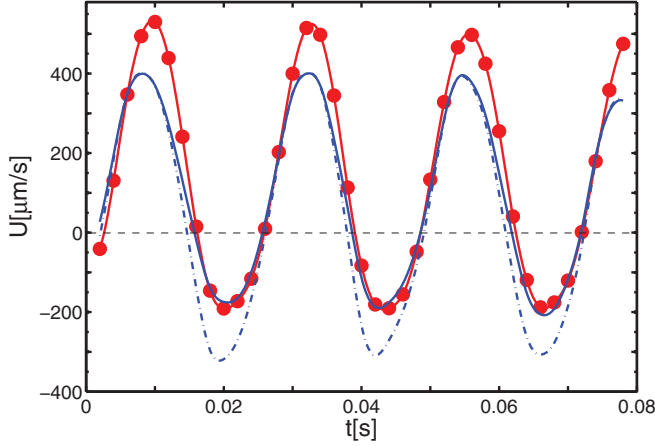
FIG. 3. (Color online) Comparison of measured (circles) and estimated oscillatory instantaneous velocity of the cell body. The velocity is estimated using resistive force theory (dash-dotted line) and the singularity method (solid line).

of the desynchronization event, during which the velocities along two flagella are almost anticorrelated and Δ reaches a maximum, while the body velocity is nearly zero. One of the flagella performs an extra beat during this desynchronization event, consistent with earlier observations [6,7,13].

During these desynchronization events, the cells wobble along their trajectories due to unequal torques from the two flagella. A preliminary study of about 80 freely swimming cells shows that fluctuations larger than 4 or 7 degrees occur approximately 10% or 3% of the time, with frequency decreasing exponentially with increasing angle. Therefore, substantial fluctuations are not uncommon, though only the largest ones produce phase slips and substantial angle change [6,7,12–14], observed here directly for freely swimming cells. Wobble events clearly can affect the paths taken by individual cells and may contribute to diffusion in natural environments [12–14].

IV. INVESTIGATION OF SWIMMING HYDRODYNAMICS

We now return to the general case of synchronized beating and investigate the hydrodynamic origins of forward motion in swimming *Chlamydomonas*. Figure 3 represents the instantaneous velocity of the cell centroid measured for a single *Chlamydomonas* alga over more than three consecutive stroke periods. The precise deformations of the flagella were simultaneously captured with high-speed imaging recording at 500 fps and the dimensions of this particular organism were measured as: major axis $a = 8.24 \pm 0.35 \,\mu$m, minor axis $b = 7.74 \pm 0.05 \,\mu$m and flagellar length $L = 13.0 \pm 0.8 \,\mu$m. The sign of the instantaneous velocity alternates corresponding to forward and backward motion, which is the typical signature of the power-recovery stroke.

The fluid flow around the swimming cell can be computed from the detailed parametrization of the experimentally recorded flagellar deformations. This computation allows us to compare theoretical and experimental swimming velocities and identify the origin of forward motion. Here, the Reynolds number (Re) is small and the hydrodynamics is governed by the viscosity dominated Stokes equations:

$$\nabla \cdot \boldsymbol{u} = 0, \quad -\nabla p + \mu \nabla^2 \boldsymbol{u} = \boldsymbol{0}, \tag{1}$$

subject to the boundary and equilibrium conditions

$$\boldsymbol{u} = \boldsymbol{U}_\Sigma \text{ on } \Sigma, \quad \mathbf{u} \to \boldsymbol{0} \text{ at, } \infty \tag{2}$$

$$\iint_\Sigma (\boldsymbol{\sigma} \cdot \boldsymbol{n}_\Sigma) \, d\Sigma = 0, \quad \iint_\Sigma \boldsymbol{r} \times (\boldsymbol{\sigma} \cdot \boldsymbol{n}) \, d\Sigma = 0, \tag{3}$$

where p is the pressure field, $\boldsymbol{u}$ is the velocity field, $\boldsymbol{U}_\Sigma$ is the velocity at the surface of the swimmer, $\boldsymbol{\sigma}$ is the hydrodynamic stress tensor, $\boldsymbol{r}$ is the position vector, Σ represents the surface of the swimmer, and $\boldsymbol{n}_\Sigma$ is the normal vector to the surface. Given the geometry of this swimming *Chlamydomonas* cell, these equations were solved approximately using two different semianalytical models: first, a local drag model referred to as resistive force theory (RFT) in the literature, then a singularity method (SM), which accounts to first order for nonlocal hydrodynamic interactions.

The RFT only takes into account local effects and neglects any hydrodynamic interactions between different parts of the swimmer [18]. This method is widely used [18–20] and assumes, at each point along the flagella, the local hydrodynamic force per unit length $\boldsymbol{f}(s)$ to be linear in the local velocity of the flagellum $\boldsymbol{V}(s)$. Similarly, the hydrodynamic force on the cell $\boldsymbol{F}$ is assumed to be linear in the velocity of the cell $\boldsymbol{U}$. Along the flagella, $\boldsymbol{f}(s)$ depends on two drag coefficients $C_\parallel$ and $C_\perp$, characterizing the hydrodynamic drag in the tangential and normal direction to the centerline of the flagella. Likewise, on the cell body, $\boldsymbol{F}$ depends on the drag coefficient in the direction of the major and minor axis of the ellipsoidal body $D_\parallel$ and $D_\perp$. The values for the drag coefficients on the slender flagella ($C_\parallel$, $C_\perp$) and on the ellipsoidal cell body ($D_\parallel$, $D_\perp$) can be derived analytically. In this work, we used standard expressions, which can be found in Refs. [21] and [22]. From the parametrization of the flagellar deformations, we compute the swimming velocity of the cell with the RFT model by imposing the equilibrium conditions in Eq. (3); see Fig. 3. The instantaneous velocity computed by the RFT reproduces the characteristic signature of the power-recovery strokes and alternates sign. The average velocity predicted is 67 μm s^{-1}, which is significantly lower than the 125 μm s^{-1} measured experimentally. Two main factors can explain this discrepancy. Considering first the power stroke, the maximal forward velocity measured is 35% higher than that computed by the RFT. This is likely due to the thin film flow conditions around the cells in the experiment, which differ from the 3D infinite flow conditions assumed in the RFT; see Eq. (2). The film thickness h is more than two orders of magnitude larger than flagellar radius r, so the effect of the thin film condition on the flagella is expected to be negligible [31]. However, h is only 1.5–2.0 times thicker than the diameter of the cell body. This proximity to the free boundaries will decrease significantly the drag experienced by the cell body in the experiment compared to the drag in infinite flow. This decreased drag corresponds to an increase in the measured instantaneous velocity. The drag experienced by a solid sphere moving parallel to a single free boundary located at 0.75–1.0 diameter from its center has been shown analytically to decrease by 16–20% compared to the drag in infinite flow conditions [23]. No equivalent

theory has been derived for the case of two free boundaries. One may expect, however, the drop in drag to double under these conditions, by analogy to the case of solid boundaries [23], and hence to account for the higher velocities observed experimentally compared to those obtained by the RFT. Next, we consider the recovery stroke. In this case, the magnitude of the negative velocities observed are 40% lower than estimated with the RFT. During the recovery stroke, the two flagella move closer to the cell body and the RFT is anticipated to breakdown due to significant nonlocal hydrodynamic interactions between the different parts of the microorganism.

In order to further investigate the effect of hydrodynamic interactions, we used a second method to model the flow around the swimming organism. In this model, the hydrodynamics is solved with a SM, for which singular fundamental solutions to the Stokes equations are distributed along the major axis of the ellipsoidal cell body and along the centerlines of both flagella. The singularity distribution satisfies the no-slip condition [Eq. (2)] to first order on the deforming surface. We use the singularity distributions from nonlocal slenderbody theory to represent the flagella [24] and a separate system of singularities to represent the ellipsoidal body [22]. Hydrodynamic interactions between distant parts of the flagella are modeled by the nonlocal slenderbody theory and interactions between the cell body and the flagella are taken into account via an extension to Faxéns laws for elliptical bodies [25]. Details of the method can be found in Ref. [26]. The singularity distribution and the swimming velocity of the cell body can be deduced from the equilibrium condition, Eq. (3). During the power stroke, the SM and the RFT are in close agreement (Fig. 3) and both predict forward velocities lower than those observed because of the infinite flow domain assumption; see Fig. 3. This agreement is expected since the flagella remain far from the cell body during the powerstroke and nonlocal hydrodynamic interactions are not significant. The effect of hydrodynamic interactions is most evident during the recovery stroke, when the negative backwards velocities computed with the nonlocal SM are 40% lower than those computed with the RFT. These lower backward velocities are in closer agreement with experimental observations and the average velocity computed by the singularity method is $88\ \mu\mathrm{m\,s}^{-1}$.

V. CONCLUSIONS

Comparing the instantaneous velocities obtained from the RFT and the SM with the measured velocities allows us to identify the hydrodynamic origin of the average forward velocity of swimming *Chlamydomonas*. During the recovery stroke, the RFT predicts backwards instantaneous velocities, which are nearly equal to the positive forward velocities during the power stroke. This symmetry contrasts with the experimental measurements for which the backwards velocities are significantly lower than the forward velocities. The RFT only accounts for the local hydrodynamics, for which the drag-based thrust is solely due to the anisotropy in the drag coefficients ($D_\perp > D_\parallel$) [8]. RFT with constant coefficients has been shown experimentally to be sufficient to describe the time-dependent motion of freely swimming spermatozoa [20]. For the power-recovery strokes, our analysis challenges the common view of a drag-based thrust relying solely on drag anisotropy. By accounting for hydrodynamic interactions to first order, the implemented SM obtains lower negative backward velocities during the recovery stroke than the RFT, in agreement with experimental observations. This allows us to identify hydrodynamic interactions between cell body and flagella as a significant contributing mechanism to forward motion.

Our results contrast with a recent RFT analysis [27] of propulsive forces on the flagellum of *Chlamydomonas*. In that work, flagellar waveforms were studied on mutant uniflagellate cells in which the beating of a single flagellum causes the cell body to spin like a top (cf. Fig. 1 of Ref. [27]). Because of greater distance between the flagellum and cell body on the return stroke (cf. Fig. 4 of Ref. [27]) in this unusual geometry, their data were adequately described by an RFT model. We show this is not the case for freely swimming, biflagellate *Chlamydomonas* cells, where RFT (which cannot account for hydrodynamic effects) does not describe well the measured cell body velocity on the return stroke when the flagella pass very close to the cell body (Fig. 1). However, a singularity model that accounts for these hydrodynamic interactions agrees well with our return stroke data, demonstrating that the cell uses these interactions to enhance net forward motion, offering new insight into the mechanics of freely swimming cells.

ACKNOWLEDGMENTS

[1] J. S. Guasto, R. Rusconi, and R. Stocker, Annu. Rev. Fluid Mech. **44**, 373 (2012).

[2] C. J. Brokaw, Math. Biosci. **90**, 247 (1988).

[3] I. R. Gibbons, J. Cell Biol. **91**, 107 (1981).

[4] G. Novarino, N. Akizu, and J. G. Gleeson, Cell **147**, 70 (2011).

[5] E. H. Harris, *The Chlamydomonas Sourcebook* (Academic Press, Oxford, 1999).

[6] U. Rüffer and W. Nultsch, Cell Motil. **5**, 251 (1985).

[7] U. Rüffer and W. Nultsch, Cell Motil. Cytoskel. **41**, 297 (1998).

[8] E. Lauga and T. R. Powers, Rep. Prog. Phys. **72**, 096601 (2009).

[9] A. Hamel, C. Fisch, L. Combettes, P. Dupuis-Williams, and C. N. Baroud, Proc. Natl. Acad. Sci. USA **108**, 7290 (2011).

[10] D. Tam and A. E. Hosoi, Proc. Natl. Acad. Sci. USA **108**, 1001 (2011).

[11] J. S. Guasto, K. A. Johnson, and J. P. Gollub, Phys. Rev. Lett. **105**, 168102 (2010).

[12] M. Polin, I. Tuval, K. Drescher, J. P. Gollub, and R. E. Goldstein, Science **325**, 487 (2009).

[13] R. E. Goldstein, M. Polin, and I. Tuval, Phys. Rev. Lett. **103**, 168103 (2009).

[14] S. Rafai, L. Jibuti, and P. Peyla, Phys. Rev. Lett. **104**, 098102 (2010).

[15] See Supplemental Material at http://link.aps.org/supplemental/10.1103/PhysRevE.88.013015 for movies of flagellar waveforms.

[16] P. V. Bayly, B. L. Lewis, P. S. Kemp, R. B. Pless, and S. K. Dutcher, Cytoskeleton **67**, 56 (2010).

[17] S. Camalet and F. Jülicher, New. J. Phys. **24**, 1 (2000).

[18] J. Gray and G. J. Hancock, J. Exp. Biol. **32**, 802 (1955).

[19] J. Lighthill, SIAM Rev. **18**, 161 (1976).

[20] B. M. Friedrich, I. H. Riedel-Kruse, J. Howard, and F. Jülicher, J. Exp. Biol. **213**, 1226 (2010).

[21] R. Cox, J. Fluid Mech. **44**, 791 (1970).

[22] A. T. Chwang and T. Y.-T. Wu, J. Fluid Mech. **67**, 787 (1975).

[23] H. Brenner, J. Fluid Mech. **12**, 35 (1962).

[24] J. Keller and S. Rubinow, J. Fluid Mech. **75**, 705 (1976).

[25] J. Happel and H. Brenner, *Low Reynolds Number Hydrodynamics* (Noordhoff International Publishing, Leyden, 1973).

[26] D. Tam, Ph.D. thesis, MIT, 2008.

[27] P. V. Bayly, B. L. Lewis, E. C. Ranz, R. J. Okamoto, R. B. Pless, and S. K. Dutcher, Biophys. J. **100**, 2716 (2011).

[28] V. Prasad and E. R. Weeks, Phys. Rev. Lett. **102**, 178302 (2009).

[29] H. Kurtuldu, J. S. Guasto, K. A. Johnson, and J. P. Gollub, Proc. Natl. Acad. Sci. USA **108**, 10391 (2011).

[30] A. J. Levine, T. B. Liverpool, and F. C. MacKintosh, Phys. Rev. E **69**, 021503 (2004).

[31] An estimate can be made based on the ratio of flagellar radius to the film thickness [28]. Alternatively, an effective 2D membrane viscosity can be computed from the Safmann-Delbruck formula [28] for the measured effective particle diffusivity in the film [29]. This gives an estimate of the hydrodynamic length scale l [30]. Comparing the ratio $L/l \sim 0.1$ with the findings of Levine *et al*. [30], the flagellar drag coefficients in the film are close to those used in the present study.